Black: referee's comments red: authors' answers
First of all, we want to thank the referee 3 for the detailed analysis of our paper.
For the details, please look into the paper with keeping track of changes.

Anonymous Referee #3

General comments: This is a carefully done study and the data is very valuable, but the preliminary data analysis and discussion have been done. What the main purpose of this study is? What's the main influencing mechanism of CO2? are there some differences with other big cites or megaregions?
Thanks for your suggestions.

The paper is aim to describe the spatial and temporal variations of CO_2 mole fractions in urban, suburban and rural areas of North China. And these measurements in and around cities are very useful for the climate and air pollution studies.
As is discussed in the paper, all the CO_2 variations at the three sites are influenced by the boundary layer height (BLH), photosynthesis and human activities. Generally, the increase of the BLH after sunrise and the photosynthetic uptake during the day make the CO_2 mole fraction decrease, but the BLH decreasing after sunset results into the accumulation of CO_2. However, at BJ, high CO_2 is more influenced by local human activities, and the CO_2 with the wind coming from the southwest is about ~21 ppm larger than those with the wind coming from the northwest during the day. At XL, besides the more significant impact of local photosynthesis, the wind from the cities in the south, such as Beijing and Tianjin, also makes CO_2 increase during the day.
In the revised paper, we add the CO_2 measurements at five urban sites in USA with a similar latitude of BJ. All these five sites belong to the CO_2 Urban Synthesis and Analysis (CO2-USA) Data Synthesis Network (Feng et al., 2016). The site locations, elevations, inlet heights, and references are listed in Table 1. As the CO_2 measurements at these five sites do not cover the period between October 2018 and September 2019, we use the latest 1-year available CO_2 measurements.

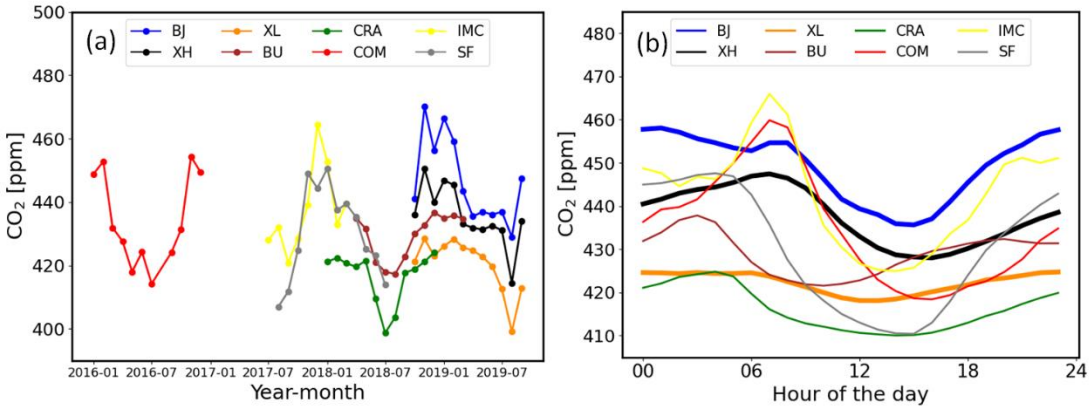

Figure 1. (a) Monthly means of CO_2 at BJ (L1), XH (L1), XL between October 2018 and September 2019, at BU, CRA, COM, IMC and SF during the latest 1 year and (b) the diurnal cycles of CO_2.

The monthly means and diurnal cycles of CO_2 at BJ (L1), XH (L1), XL, and 5 American urban sites

are shown in Figure 1. It is found that the phases of the seasonal CO_2 cycles at BU, CRA, COM, IMC and SF are consistent with the observations at BJ (L1), XH (L1) and XL, with a high value in autumn-winter and a low value in summer. Among the five American sites, the highest CO_2 concentration is observed at IMC. The IMC site is inside a commercial zone and the CO_2 measurements over there are more strongly influenced by local emissions over there (Bares et al., 2019). The CO_2 concentration is also high at COM, because the Los Angeles megacity is one of the largest fossil fuel CO_2 emitters in the world (Matthäus et al., 2021). Figure 1 (a) shows that the CO_2 concentrations at COM and IMC are in the same level with the one at XH, but are less than the CO_2 concentration at BJ. The CO_2 concentrations at SF, BU and CRA are much lower as compared to BJ, because of lower anthropogenic emissions at these sites (McKain et al., 2015; Lauvaux et al., 2016; Shusterman et al., 2016).

Figure 1 (b) shows the diurnal variations of CO_2, with the amplitudes of 22.4, 19.4, 6.6, 16.3, 14.8, 41.5, 41.1 and 37.2 ppm at BJ (L1), XH (L1), XL, BU, CRA, COM, IMC and SF, respectively. The amplitudes of the diurnal variation at COM, IMC and SF are higher than that at BJ, although the yearly mean CO_2 levels at these sites are smaller than that at BJ. As the sampling heights at these sites and BJ are similar, the large amplitudes of the diurnal variation indicate that stronger variation in the local emissions and/or sinks exists at these three American sites as compared to BJ.

Table 1. Site characteristics of BJ, XH and XL in North China, BU, CRA, COM, IMC and SF in USA from the CO_2 Urban Synthesis and Analysis (CO2-USA) Data Synthesis Network.

Site Code	Site Name	Lat (°N)	Lon (°E)	Elevation (m a.s.l.)	Inlet Height (m a.g.l.)	City	Reference
BJ	Beijing	39.96	116.36	49	80/280	Beijing	Cheng et al., 2018
XH	Xianghe	39.75	116.96	30	60/80	Xianghe	Yang et al., 2020
XL	Xinglong	40.40	117.50	940	10	Xinglong	Yang et al.,2019
BU	Boston University	42.35	-71.10	4	29	Boston	Sargent et al., 2018 McKain et al., 2015
CRA	Crawfordsville	39.99	-86.74	264	76	Indianapolis	Lauvaux et al., 2016 Richardson et al., 2017
COM	Compton	33.87	-118.28	9	45	Los Angeles	Verhulst et al., 2017
IMC	Intermountain Medical Center	40.67	-111.89	1316	66	Salt Lake City	Mitchell et al., 2018 Bares et al., 2019
SF	SF Hospital Bldg 5	37.76	-122.41	23.9	52	San Francisco	Shusterman et al., 2016

Specific comments:

1. Please explain the data processing method and the proportion of valid data at the three sites.

Thanks for your suggestions. More information about the data processing method is added in the revised paper.

(1) Calibration

The intake system is connected to an 8-position valve, which is used to choose the air coming from the sample air, the target gas, or the calibration gas. The target and calibration gases are pressurized

in 29.5 L treated aluminum alloy cylinders, which are scaled to the WMO X2007 standard by the China Meteorological Administration, Meteorological Observation Centre. The same calibration procedure is operated at these three sites: 1) 3-hours sample air; 2) 5-minutes calibration gas; 3) 3-hours sample air; 4) 5-minutes target gas. This process repeats every 6 hours and 10 minutes. Note that, the airs coming from two levels at XH and BJ are switched every 5 minutes during the 3-hours sample air period. As the remaining volume in the tubes needs time for flushing, the response of the analyzer turns to be stable about 1 minute after each switching. In order to reduce the uncertainty, we do not consider the first 3-minutes measurements after each switching.

The calibration gas is to calculate the calibration factor (*cf*),

$$cf = CO_{2,mcal}/CO_{2,cal} \quad (1)$$

where $CO_{2,mcal}$ is the CO_2 mole fraction measured by the Picarro analyzer from the calibration gas and $CO_{2,cal}$ is the standard CO_2 mole fraction of the calibration cylinder.

The target gas is used to check the precision and stability of the system. The T value are calculated as follows,

$$T = cf \times CO_{2,mtar} - CO_{2,tar} \quad (2)$$

where $CO_{2,tar}$ is the standard CO_2 mole fraction of the target gas cylinder, $CO_{2,mtar}$ is the CO_2 mole fraction measured by the Picarro analyzer from the target gas, cf is calculated from the CO_2 mole fraction measured by the Picarro analyzer from the calibration gas.

To keep the CRDS stable over time, only the periods with T value within ±0.1 ppm are selected. The measurement uncertainties of the Picarro instrument at the three sites are calculated as the standard deviation (std) of T, which are 0.01, 0.06, and 0.02 ppm at BJ, XH, and XL respectively.

(2) Data Processing

Besides the calibration procedure, we also do auto and manual flagging of the raw data. In each 1-hour CO_2 measurement window, auto-flags are assigned when deviations from CO_2 mean are found larger than 2-times hourly CO_2 std. Furthermore, manual flags are assigned by technicians at each site according to the logbook to exclude no-valid data resulted from the inlet filter, pump, and extreme weather issues. In addition, as the CRDS measurement system records CO_2 and CH_4 simultaneously, the variations of these two gases are checked together to manually flag CO_2/CH_4 outliers.

The proportions of valid data are 98.5% and 99.1% at BJ L1 and L2, 99.3% and 99.1% at XH L1 and XH L2, 99.9% at XL.

All these information has been added in the revised version.

2. As CO_2 at XL is regarded as the background in this study, please explain whether there is a special data processing method for it, because the observational data at XL include not only the background information, but also local information about natural ecosystem and human activity, especially, the intake system of XL is on the roof.

Thanks for your suggestions.

In this study, we treat the CO_2 measurements at XL as the background of BJ and XH. In the revised paper, we use the CarbonTracker model, version CT-NRT.v2021-3 (Peters et al., 2005) to evaluate the influence of anthropogenic, biogenic, oceanic and fire sources at these three sites. The CarbonTracker is a data assimilation system developed by the National Oceanic and Atmospheric

Administration (NOAA) to keep track of sources and sinks of atmospheric CO_2 around the world. Four tracers (biosphere, ocean, fire and fossil fuel) are treated separately to simulate atmospheric CO_2 mole fractions. Mustafa et al. (2020) evaluated the CarbonTracker model in Asia by comparing with satellite measurements, and they found that the CarbonTracker model captures the variation of CO_2 well. The model provides 3-hourly CO_2 data at 25 levels from surface to ~ 123 km, and the spatial resolution of the global CarbonTracker CO_2 simulation is 3°×2° (longitude x latitude). As BJ and XH are in the same model grid, we note the CO_2 simulations in the BJ/XH grid as BJ.

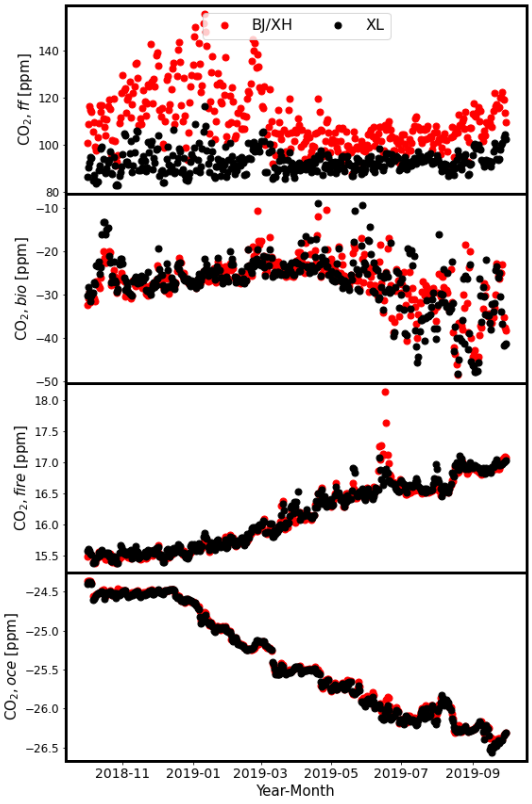

Figure 2. The time series of CO_2 simulations from fossil fuel ($CO_{2,ff}$), biosphere ($CO_{2,bio}$), fire ($CO_{2,fire}$) and ocean ($CO_{2,oce}$) modules at BJ/XH and XL.

Figure 2 shows the time series of CO_2 simulations from fossil fuel ($CO_{2,ff}$), biosphere ($CO_{2,bio}$), fire ($CO_{2,fire}$) and ocean ($CO_{2,oce}$) modules at BJ/XH and XL between October 2018 and September 2019. It is found that the fire and ocean CO_2 at BJ/XH and XL are close to each other throughout the whole year. The biogenic CO_2 at BJ/XH and XL have a similar level between October 2018 and June 2019, and become slightly different in summer 2019. However the difference in biogenic CO_2 is much less than that of the anthropogenic CO_2 differences. The variation of the fossil fuel CO_2 at XL is much less than that at BJ/XH. Therefore, by using the CO_2 measurements at XL as the background, we can significantly reduce the influence from fire, biosphere and ocean, and extract the signal of the anthropogenic CO_2 differences.

3. It is very pity that there are no meteorological parameters at XH. For the situation (2.1) and the meteorological field (2.3), it seems the air masses from BJ can be captured much more at XH because “the percentage of wind frequency in the north region is 34%, 36%, 50% and 60%

respectively from spring to winter". And the air masses can be captured at XL only when the wind comes from SW.

Thanks for your the comment on this issue.

We are now devoting to fix the meteorology sensor at XH, which may provide more meteorological information in the future study.

References

Bares, R., Mitchell, L., Fasoli, B., Bowling, D. R., Catharine, D., Garcia, M., Eng, B., Ehleringer, J., and Lin, J. C.: The Utah urban carbon dioxide (UUCON) and Uintah Basin greenhouse gas networks: instrumentation, data, and measurement uncertainty, Earth Syst. Sci. Data., 11, 1291–1308, https://doi.org/10.5194/essd-11-1291-2019, 2019.

Cheng, X. L., Liu, X. M., Liu, Y. J., and Hu, F.: Characteristics of CO2 Concentration and Flux in the Beijing Urban Area, J. Geophys. Res. Atmos., 123, 1785–1801, https://doi.org/10.1002/2017JD027409, 2018.

Feng, S., Lauvaux, T., Newman, S., Rao, P., Ahmadov, R., Deng, A., Díaz-Isaac, L. I., Duren, R. M., Fischer, M. L., Gerbig, C., Gurney, K. R., Huang, J., Jeong, S., Li, Z., Miller, C. E., O'Keeffe, D., Patarasuk, R., Sander, S. P., Song, Y., Wong, K. W., and Yung, Y. L.: Los Angeles megacity: a high-resolution land–atmosphere modelling system for urban CO2 emissions, Atmos. Chem. Phys., 16, 9019–9045, https://doi.org/10.5194/acp-16-9019-2016, https://acp.copernicus.org/articles/16/9019/2016/, 2016.

Lauvaux, T., Miles, N. L., Deng, A., Richardson, S. J., Cambaliza, M. O., Davis, K. J., Gaudet, B., Gurney, K. R., Huang, J., O'Keefe, D., Song, Y., Karion, A., Oda, T., Patarasuk, R., Razlivanov, I., Sarmiento, D., Shepson, P., Sweeney, C., Turnbull, J., and Wu, K.: Highresolution atmospheric inversion of urban CO2 emissions during the dormant season of the Indianapolis Flux Experiment (INFLUX), J. Geophys. Res. Atmos., 121, 5213–5236, https://doi.org/10.1002/2015JD024473, 2016.

Matthäus, K., Annmarie, E., Dustin, R., Lin, J., Feng, S., Lei, R. X., Lauvaux, T., Oda, T., Roehl, C., Blavier, J. F., and Iraci, L.: Urbanfocused satellite CO2 observations from the Orbiting Carbon Observatory-3: A first look at the Los Angeles megacity, Remote Sens. Environ., 258, 112 314, https://doi.org/10.1016/j.rse.2021.112314, 2021.

McKain, K., Down, A., Raciti, S. M., Budney, J., Hutyra, L. R., Floerchinger, C., Herndon, S. C., Nehrkorn, T., Zahniser, M. S., Jackson, R. B., Phillips, N., and Wofsy, S. C.: Methane emissions from natural gas infrastructure and use in the urban region of Boston, Massachusetts, Proc. Natl. Acad. Sci. U. S. A., 112, 1941–1946, https://doi.org/10.1073/pnas.1416261112, 2015.

Mitchell, L. E., Lin, J. C., Bowling, D. R., Pataki, D. E., Strong, C., Schauer, A. J., Bares, R., Bush, S. E., Stephens, B. B., Mendoza, D., Mallia, D., Holland, L., Gurney, K. R., and Ehleringer, J. R.:

Long-term urban carbon dioxide observations reveal spatial and temporal dynamics related to urban characteristics and growth, Proc. Natl. Acad. Sci. U. S. A., 115, 2912–2917, https://doi.org/10.1073/pnas.1702393115, 2018.

Mustafa, F., Bu, L. B., Wang, Q., Ali, M. A., Bilal, M., Shahzaman, M., and Qiu, Z. F.: Multi-Year Comparison of CO2 Concentration from NOAA Carbon Tracker Reanalysis Model with Data from GOSAT and OCO-2 over Asia, Rem. Sens., 12, 2498, https://doi.org/10.3390/rs12152498, 2020.

Peters, W., Miller, J. B., Whitaker, J., Denning, A. S., Hirsch, A., Krol, M. C., Zupanski, D., Bruhwiler, L., and Tans, P. P.: An ensemble data assimilation system to estimate CO2 surface fluxes from atmospheric trace gas observations, J. Geophys. Res. Atmos., 110, https://doi.org/10.1029/2005JD006157, 2005.

Richardson, S. J. and Miles, N. L., Davis, K. J., Lauvaux, T., Martins, D. K., Turnbull, J. C., McKain, K., Sweeney, C., and L., M. O.: Tower measurement network of in-situ CO2, CH4, and CO in support of the Indianapolis FLUX (INFLUX) Experiment., Elementa: Science of the Anthropocene, 5, 59, https://doi.org/10.1525/elementa.140, 2017.

Sargent, M., Barrera, Y., Nehrkorn, T., Hutyra, L. R., Gately, C. K., Jones, T., McKain, K., Sweeney, C., Hegarty, J., Hardiman, B., Wang, J. A., and Wofsy, S. C.: Anthropogenic and biogenic CO2 fluxes in the Boston urban region, Proc. Natl. Acad. Sci. U. S. A., 115, 7491–7496, https://doi.org/10.1073/pnas.1803715115, 2018.

Shusterman, A. A., Teige, V. E., Turner, A. J., Newman, C., Kim, J., and Cohen, R. C.: The BErkeley Atmospheric CO2 Observation Network: 480 initial evaluation, Atmos. Chem. Phys., 16, 13 449–13, https://doi.org/10.5194/acp-16-13449-2016, 2016.

Verhulst, K. R., Karion, A., Kim, J., Salameh, P. K., Keeling, R. F., Newman, S., Miller, J., Sloop, C., Pongetti, T., Rao, P., Wong, C., Hopkins, F. M., Yadav, V., Weiss, R. F., Duren, R. M., and Miller, C. E.: Carbon dioxide and methane measurements from the Los Angeles Megacity Carbon Project – Part 1: calibration, urban enhancements, and uncertainty estimates, Atmos. Chem. Phys., 17, 8313–8341, https://doi.org/10.5194/acp-17-8313-2017, 2017.

Yang, Y., Zhou, M., Langerock, B., Sha, M. K., Hermans, C., Wang, T., Ji, D., Vigouroux, C., Kumps, N., Wang, G., De Mazière, M., and Wang, P.: New ground-based Fourier-transform near-infrared solar absorption measurements of XCO2, XCH4 and XCO at Xianghe, China, Earth Syst. Sci. Data., 12, 1679–1696, https://doi.org/10.5194/essd-12-1679-2020, 2020.

Yang, Y., Wang, T., Wang, P. C., Zhou, M. Q., and Yao, B.: In-situ measurement of CO2 at the Xinglong regional background station over North China, Atmospheric and Oceanic Science Letters, 12, 385–391, https://doi.org/10.1080/16742834.2019.1644949, 2019.